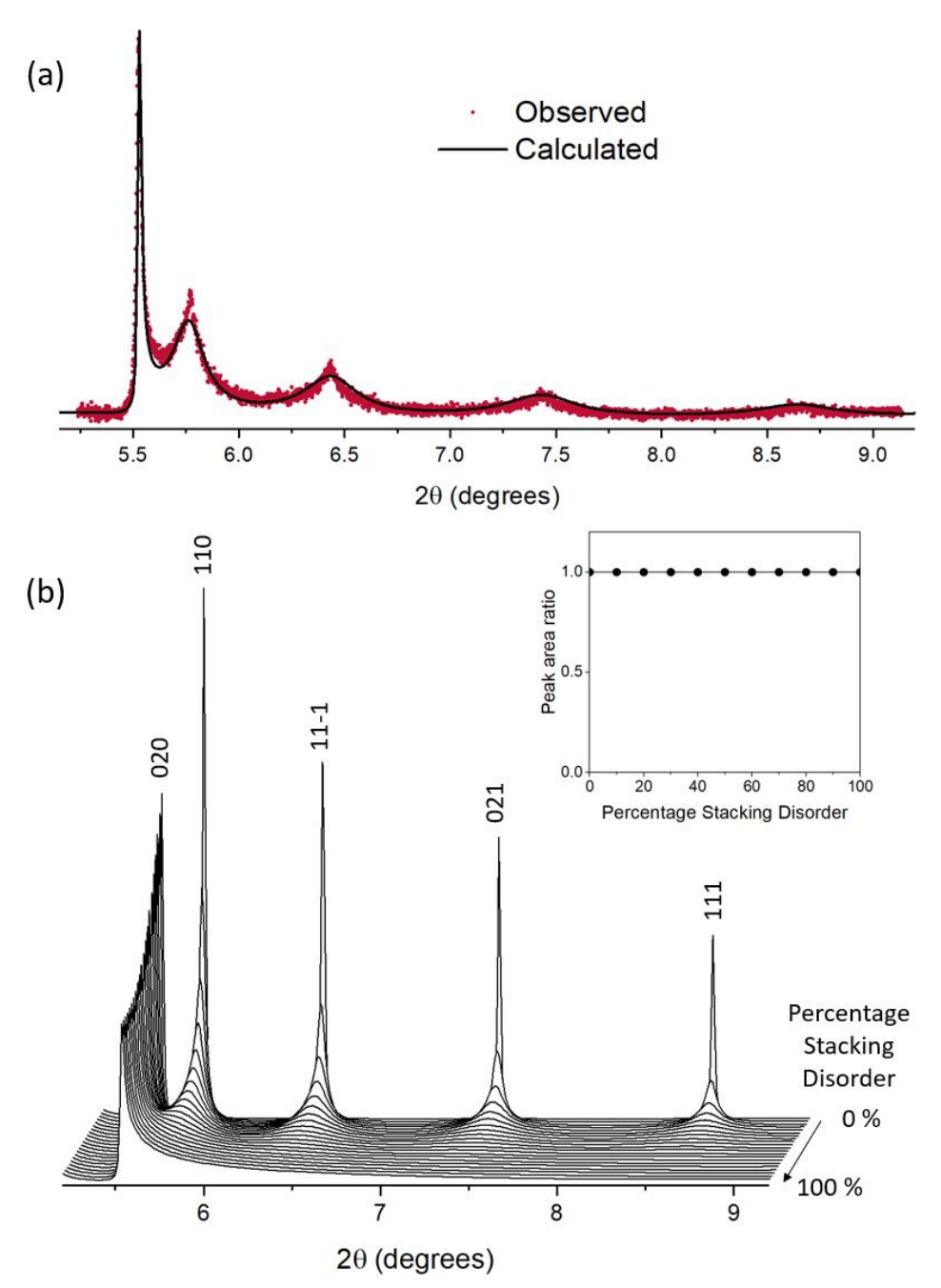


Atom	Wyckoff Positions	х	У	Z	Occupancy	U _{iso}
Li	3a	0.0	0.0	0.0	1.0	0.0115(6)
Li	3b	0.0	0.0	0.5	0.2	0.0115(6)
Ni / Co / Mn	3b	0.0	0.0	0.5	0.13/0.13/0.54	0.0043(1)
0	6c	0.0	0.0	0.2409(1)	1.0	0.0109(2)

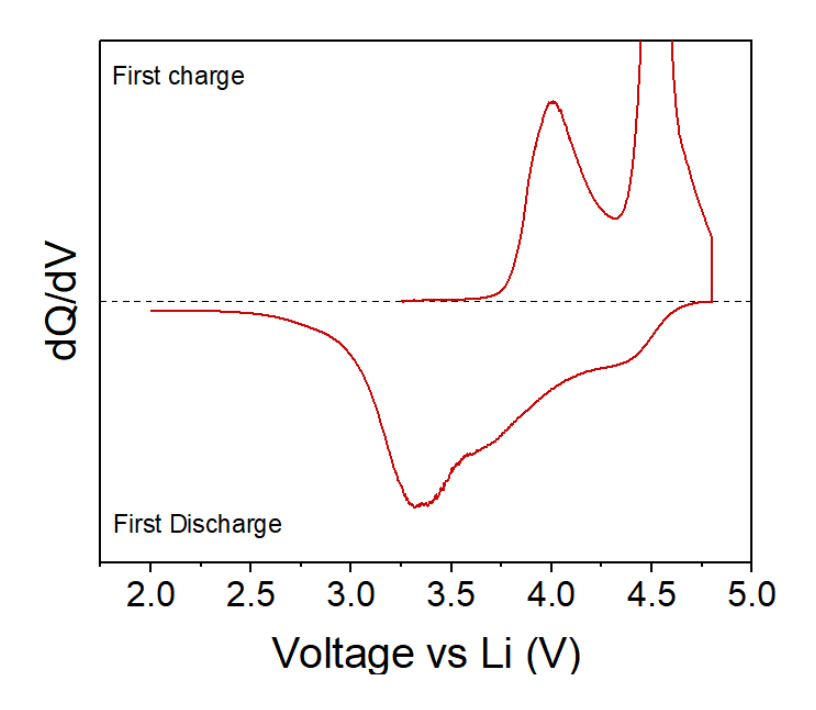
Space Group $R\overline{3}m$, a = 2.8591(1), c = 14.2764(1) $R_w = 13.4$, $R_{exp} = 4.39$

Composition from ICP-OES: $Li_{1.19(1)}Ni_{0.14(1)}Co_{0.13(1)}Mn_{0.54}O_2$

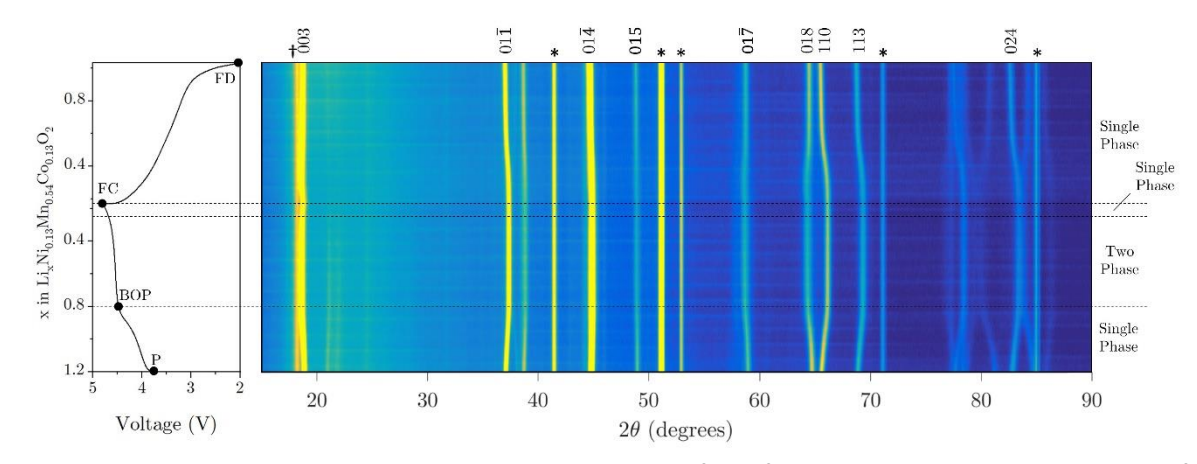
Supplementary Figure 1. Rietveld Refinement and Parameters of synchrotron powder X-ray diffraction data for $Li_{1.2}Ni_{0.13}Co_{0.13}Mn_{0.54}O_2$ collected from 11BM, Advanced Photon Source, Argonne National Lab.



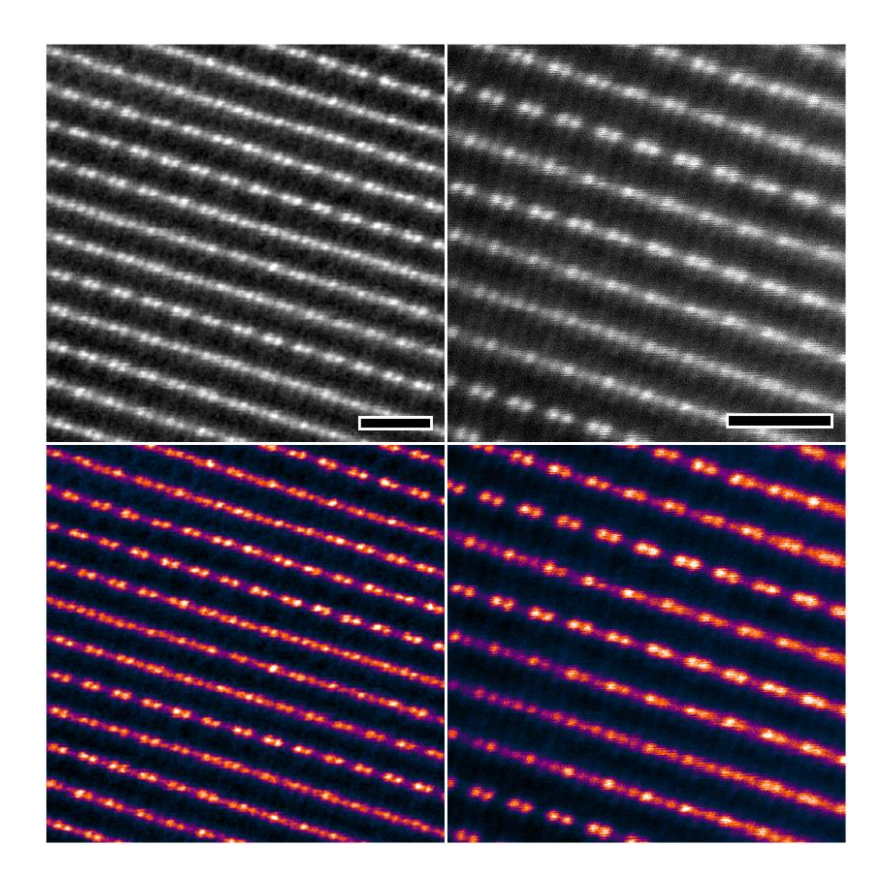
Supplementary Figure 2. Stacking Faults Analysis (a) Stacking faults analysis for pristine $Li_{1.2}Ni_{0.13}Co_{0.13}Mn_{0.54}O_2$ demonstrating 20% stacking faults. (b) Increasing stacking disorder results in asymmetric peak broadening, however, there is no decrease in the peak area ratio between the superstructure peaks and the 001 (inset). In contrast, increasing disorder due to in-plane TM migration necessarily leads to a decrease in peak area due to the averaging of X-ray structure factors between the 2b and the 4g sites.



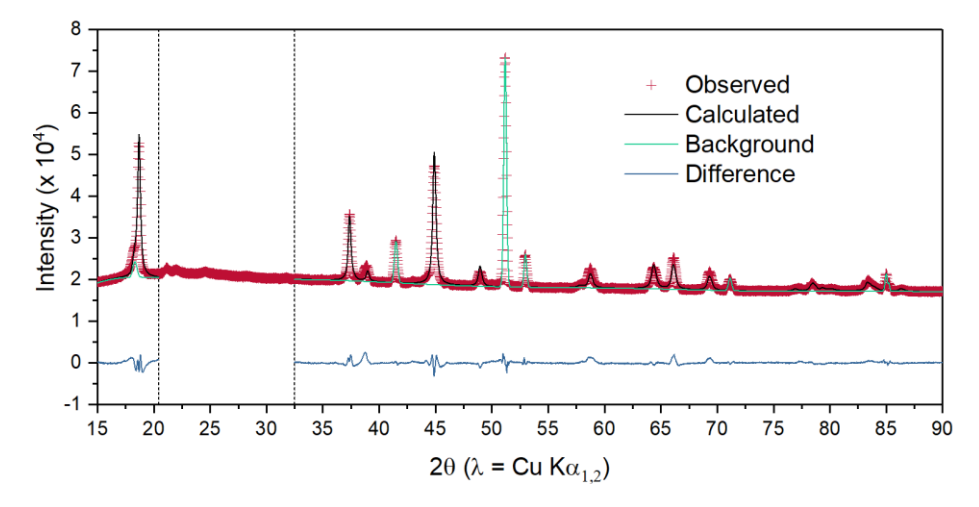
Supplementary Figure 3. dQ/dV plot for $Li_{1.2}Ni_{0.13}Co_{0.13}Mn_{0.54}O_2$ at 20 mA g^{-1} . The peak at around 4.5 V on discharge has been discussed several times before and is ascribed to TM reduction.



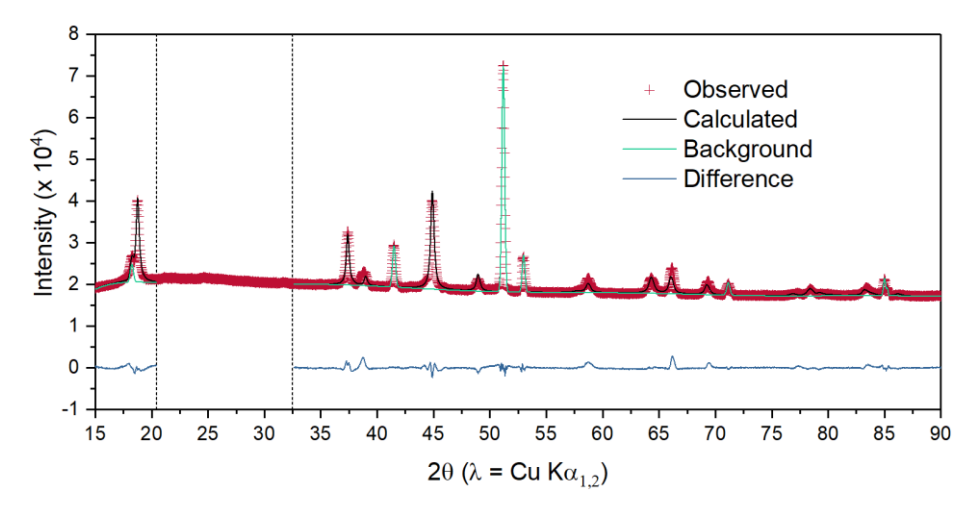
Supplementary Figure 4. Operando PXRD data for first charge-discharge cycle of $Li_{1.2}Ni_{0.13}Co_{0.13}Mn_{0.54}O_2$ charged at 10 mAg⁻¹. Peaks marked with '*' arise from the operando cell used, and '†' from the PTFE binder used in the electrode.



Supplementary Figure 5. HAADF-STEM images for fully discharged $Li_{1.2}Ni_{0.13}Co_{0.13}Mn_{0.54}O_2$ showing some regions of ordering in the midst of extensive and dominant disordering. There is clear resolution between single atomic columns indicating the loss of dumbbells is not a result of strain but rather TM migration. 1 nm scale bars.

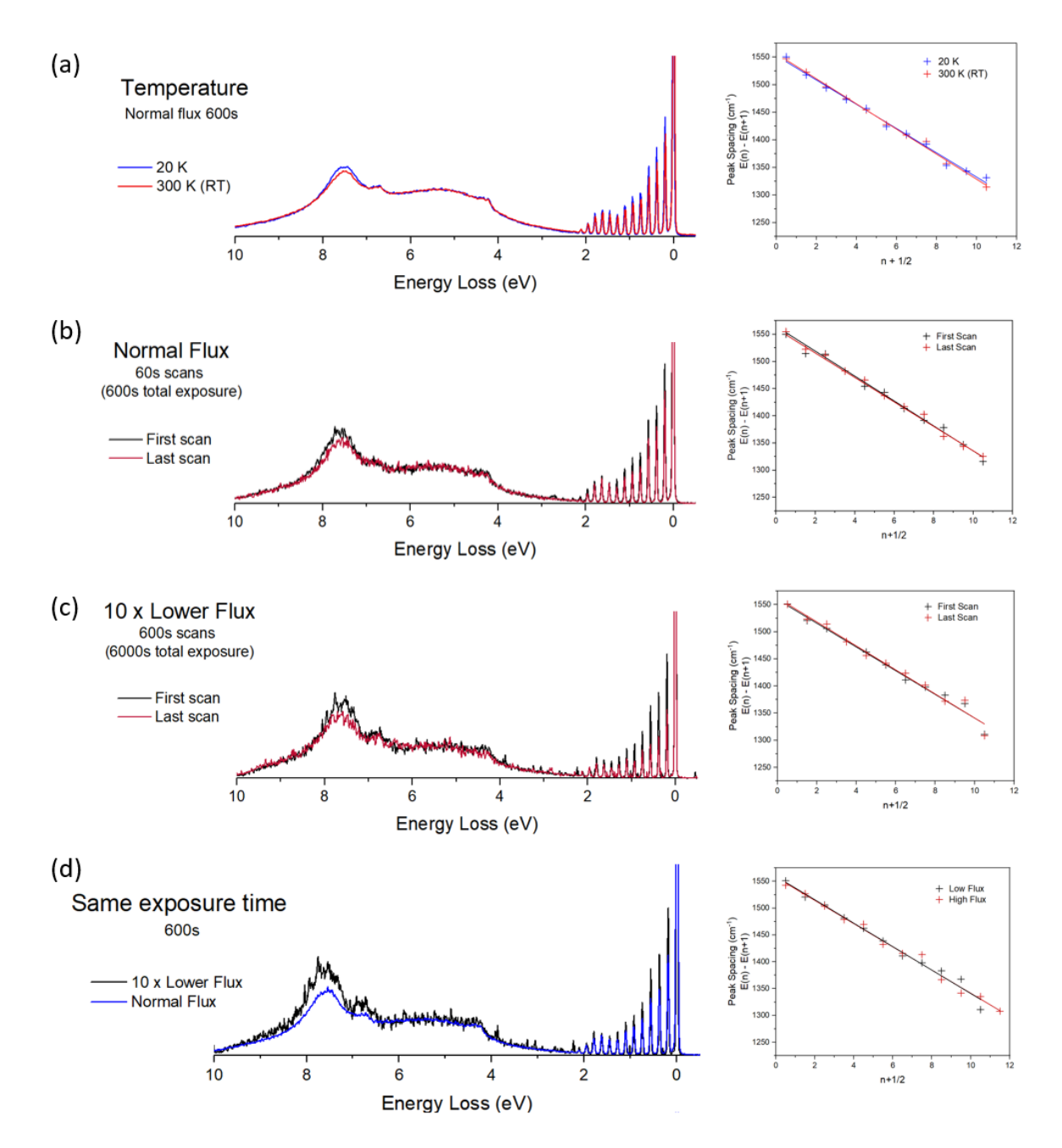


Atom	Wyckoff Positions	Х	у	Z	Occupancy	
Li / Ni*	3a	0.0	0.0	0.0	0.8 / 0.004	
Li / Ni / Co / Mn	3b	0.0	0.0	0.5	0.0 / 0.126 / 0.13 / 0.54	
0	6c	0.0	0.0	0.2458(1)	1.0	
Space Group R $\overline{3}$ m, a = 2.8334(2), c = 14.398(2), χ^2 = 2.87						

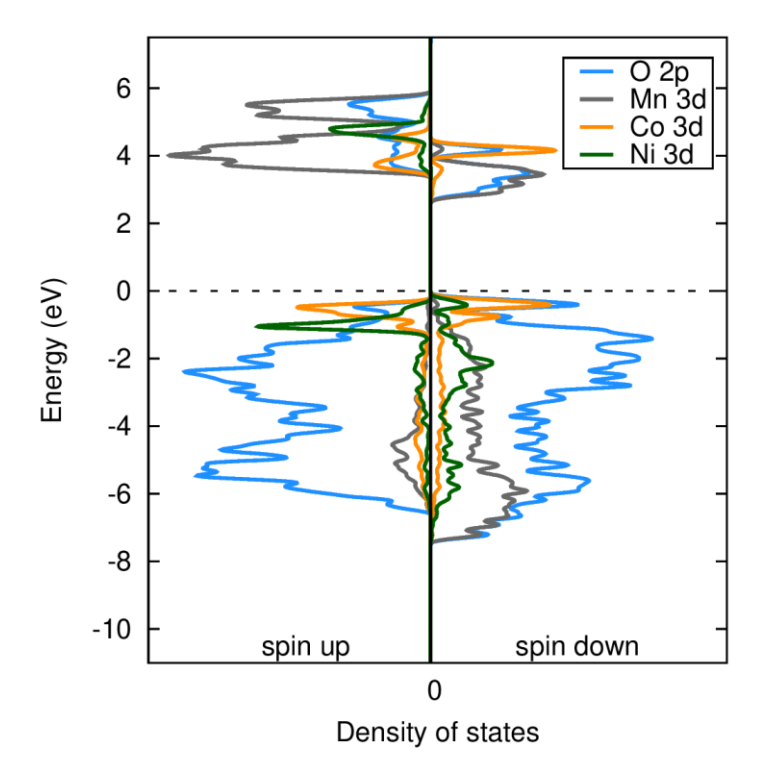


Atom	Wyckoff Positions	Х	У	Z	Occupancy	
Li / Ni*	3a	0.0	0.0	0.0	0.15 / 0.068	
Li / Ni / Co / Mn	3b	0.0	0.0	0.5	0.0 / 0.062 / 0.13 / 0.54	
0	6c	0.0	0.0	0.2476(3)	1.0	
Space Group R $\overline{3}$ m, a = 2.8357(3), c = 14.387(2), χ^2 = 2.75						

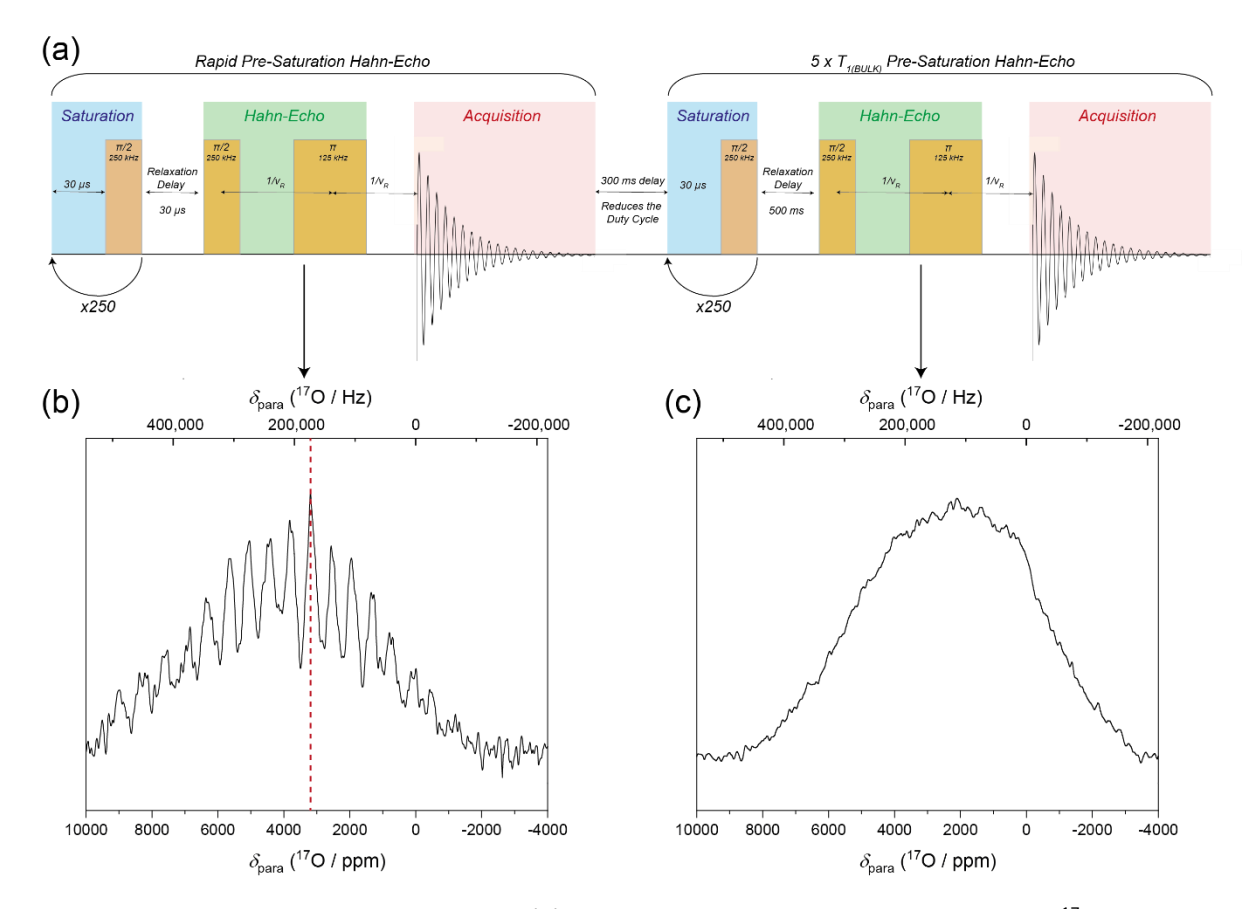
Supplementary Figure 6. Rietveld refinement of operando XRD data at the beginning of plateau (BOP), upper panel, and full charge (FC), lower panel. Peaks were fitted to the PTFE and operando cell window to account for background scattering (green line). U_{iso} values were all set to 0.01. *Ni is used to represent all TM species since XRD cannot distinguish between them.



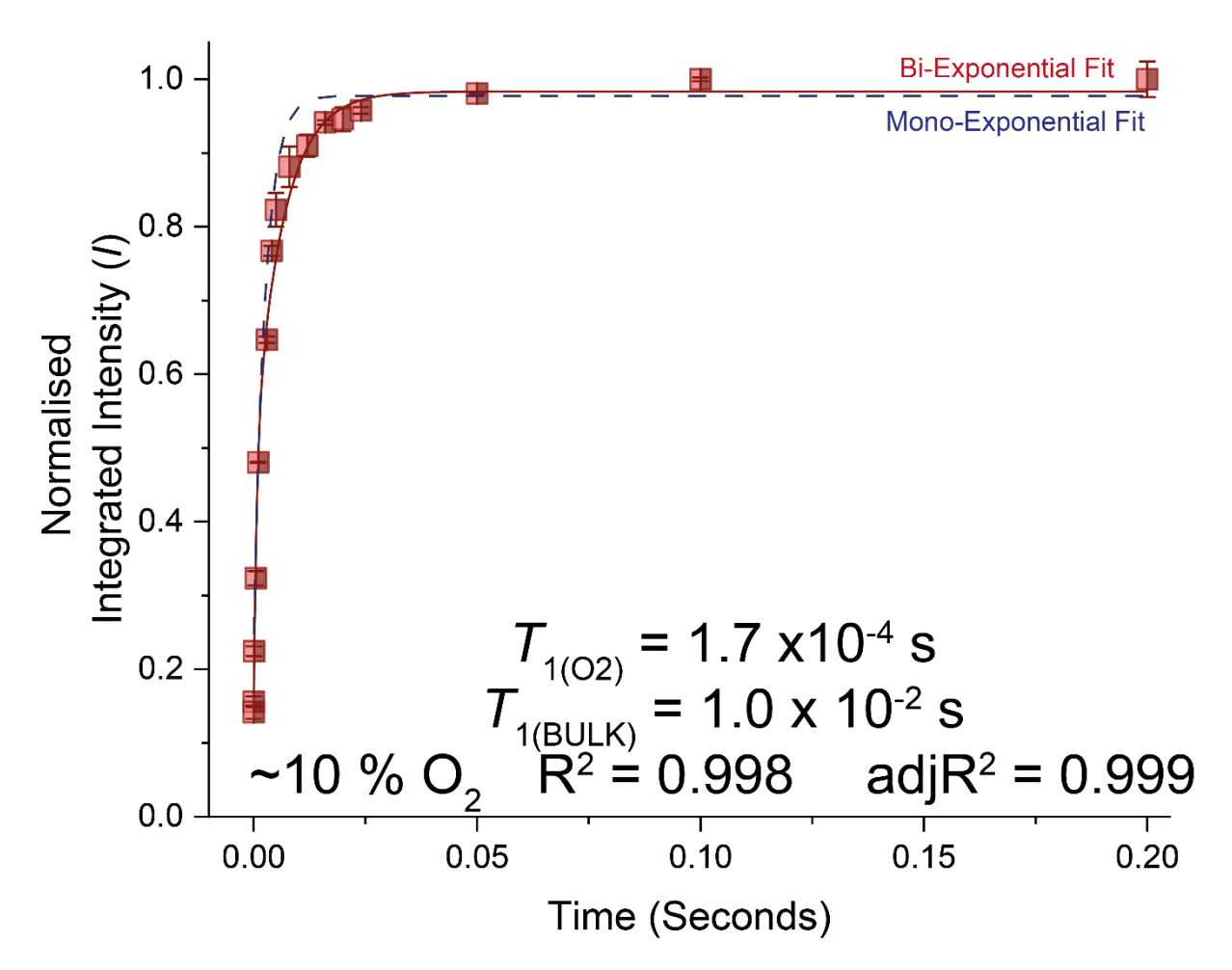
Supplementary Figure 7. High-resolution RIXS Spectra under different temperature and X-ray beam flux conditions. (a) Samples measured at 300 K and 20 K at normal flux for a total of 600s. (b) and (c) Spectra acquired at 20K before and after prolonged beam exposure at normal flux (10^{12} ph s⁻¹) and 10x lower flux (10^{11} ph s⁻¹) respectively. (d) Direct comparison of spectra collected for equal time exposure (600s) at the different fluxes at 20K. A more intense signal for molecular O_2 is seen at lower temperature and under lower beam flux. Birge-Sponer plots for the vibrational progression measured under each condition show no change in O-O bonding.



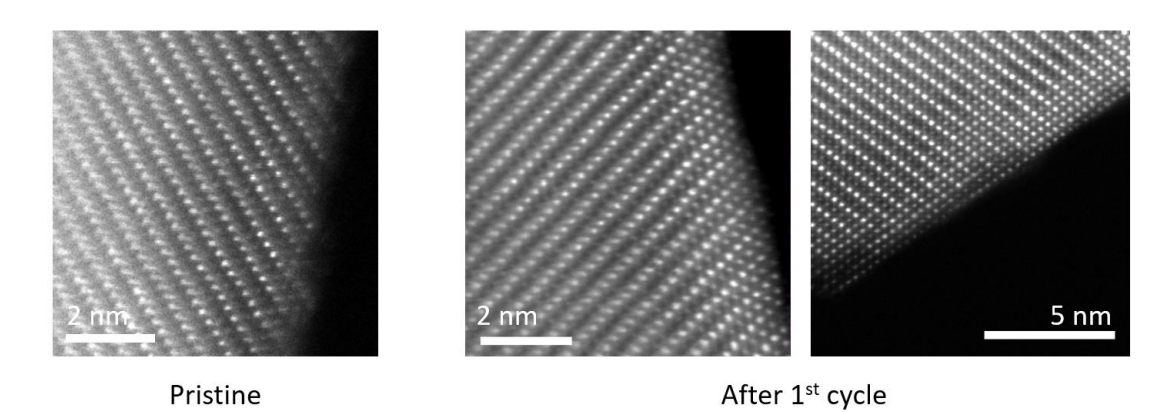
Supplementary Figure 8. Density of States plots for $Li_{1.2}Ni_{0.13}Co_{0.13}Mn_{0.54}O_2$ in the Pristine (P) state.



Supplementary Figure 9. NMR sequence (a) The interleaved pre-saturation solid state 17 O magic angle spinning (MAS) nuclear magnetic resonance (NMR) pulse sequence utilised to isolate the O_2 species. A rapid relaxation delay facilitated by pre-saturation provides a bias towards promptly relaxing paramagnetic species such as $^{17}O_2$ in the cathodes, this was interleaved with a more typical 500 ms relaxation delay pre-saturation Hahn-echo which gave a ^{17}O resonance representative of the bulk lattice oxide environments. The experiment takes advantage of the two orders of magnitude difference between the T_1 of the bulk lattice oxides ($^{\sim}17$ ms) and the intramolecular O_2 ($^{\sim}0.10$ ms). (b, c) The solid state ^{17}O MAS NMR fully charged NMC spectra using; (b) rapidly relaxing pre-saturation Hahn-echo and (c) 5 x T_1 relaxing pre-saturation Hahn-echo. The centre-band is highlighted with the (b) red dashed line and is not discernible in the (c) bulk spectra.



Supplementary Figure 10. ¹⁷**O MAS VOCS NMR** The solid state ¹⁷O MAS VOCS NMR T_1 spin-lattice relaxation of the oxygen species in Li_{1.2}Ni_{0.13}Co_{0.13}Mn_{0.54}O₂ at full charge (FC). The data was achieved using a saturation recovery sequence, as outlined in the extended methods section. The solid red line represents a bi-exponential fit, $S(t) = S_{eqa}(1-\exp^{(-t/T1BULK)}) + S_{eqb}(1-\exp^{(-t/T1O2)})$ and the dashed blue is a mono-exponential fit, $S(t) = S_{eq}(1-\exp^{(-t/T1)})$, of the data. An adjusted R² of 0.999 (compared to a R² of 0.986 for a mono-exponential fit) suggests the number of predictors used in the fit (2, bi-exponential fit) is appropriate for this dataset.



Supplementary Figure 11. HAADF-STEM images showing the formation of a densified surface structure during the first cycle.